Maximum-rapidity-gap distribution*

S. T. Jones†‡ and D. R. Snider§
High Energy Physics Division, Argonne National Laboratory, Argonne, Illinois 60439
(Received 17 September 1973)

We examine the maximum-rapidity-gap distribution as a proposed means of determining the amount of diffractive dissociation (d.d.) (Pomeron exchange) in the data. We find that a clear measurement of d.d. is not possible but that the distribution does separate into two regions where either the diffractive or nondiffractive mechanism dominates. This separation occurs at $\Delta \approx 4.0$.

I. INTRODUCTION

The precise definition and means of measuring diffractive dissociation have always been somewhat of a problem. We study the possibility of using a new quantity, the maximum-rapidity-gap distribution, as an energy-independent method of determining approximately the amount of diffractive dissociation (Pomeron exchange) in the data. This approach has been proposed by Chew and coworkers[1] and now we undertake a more serious study of it. The ideas presented here use the language of the two-component (diffractive plus nondiffractive) models, but are not at all limited to this framework.

The maximum-rapidity-gap distribution is appropriate for semiinclusive processes, where all charged particles are measured, but neutrals are summed over. For each event, the observed particles are ordered in rapidity; we define Δ to be the *largest* of the gaps in rapidity between *adjacent* particles. We then define $\sigma(\Delta)$ to be the cross section for production of final states where the maximum rapidity gap is less than or equal to Δ. $d\sigma/d\Delta$ is the corresponding differential cross section, obtained from experimental data by binning the events according to the size of the maximum gap, Δ.[2] We call $d\sigma/d\Delta$ the maximum-rapidity-gap distribution. In terms of cross sections, if $d\sigma_n/dy_1\cdots dy_n$ is the *ordered* differential cross section [where y_i is the rapidity of the ith particle, $y_i \leq y_{i+1}$, and $Y = \ln(s/m_a m_b)$], then

$$\sigma_n(\Delta) = \int_0^Y dy_1 \int_{y_1}^{y_1+\Delta} dy_2 \cdots \int_{y_{n-1}}^{y_{n-1}+\Delta} dy_n \frac{d\sigma_n}{dy_1 \cdots dy_n} \tag{1}$$

and

$$\sigma(\Delta) = \sum_n \sigma_n(\Delta) .$$

The usefulness of $\sigma(\Delta)$ is based on the idea that diffractive processes are expected to contribute mainly to large subenergies, and hence large gaps Δ, whereas nondiffractive processes should contribute little to this region. It is our purpose to illustrate by general arguments and simple models the expected shape of $d\sigma/d\Delta$ and the sort of difficulty one encounters in using it to measure the amount of diffractive dissociation at NAL and CERN ISR energies. Basically we find that there is not a clear separation of events into two groups, diffractive and nondiffractive, but that there are two regions where either mechanism dominates, although some of the other is present. Although one can be relatively sure that most of the events with large rapidity gaps, say, $\Delta > 4.5$ or 5, are Pomeron exchanges, there still may be an appreciable fraction of the Pomeron-exchange events in the region dominated by the nondiffractive contribution. The existence of an appreciable cross section at large gaps can thus be taken as independent evidence for the existence of diffractive dissociation at high energies, but determining the *amount* of diffraction is difficult.

Before discussing the results of our analysis, it is important that we have a clear definition of the term diffraction. In particular, not all dissociation is diffractive. We require in general that a diffractive mechanism (a) lead to an energy-independent cross section, and (b) correspond to exchange of no quantum numbers. That is, it corresponds to Pomeron exchange. A dissociation or fragmentation event will be one where one (or both) of the incident particles "decays" into a number of particles having, in aggregate, the same quantum numbers as the incident particle. The aggregate will also have nearly the same momentum (i.e., the momentum transfer t is typically very small). For fixed missing mass M, momentum transfer t, number of particles n, etc., the dissociation cross section is generally energy-dependent. From Regge theory we might expect to fit the cross section with

$$\frac{d^2\sigma_{ab}^n(s,t,M^2)}{dt\,dM^2} = |\beta_{aP}(t)\gamma_{bP}^n(t,M^2) + \beta_{af}(t)\gamma_{bf}^n(t,M^2)s^{-1/2}|^2 . \tag{2}$$

The energy-independent term due to Pomeron exchange we define to be *diffractive* dissociation. The cross terms and the ff terms we call nondiffractive dissociation. This means that, experimentally, one can only *decisively* determine what fraction of the dissociation cross section is diffractive by comparing results at various energies. Triple-Regge fits are an effective means of doing this (although they miss the double-diffractive dissociation).

With data in only a small energy interval, it is impractical to use the above general definition of diffraction. This has motivated us to examine an operational definition which could be useful at even a single energy and applicable on an event-by-event basis. We find that rather general physical arguments predict an approximate separation of events into two regions in $d\sigma/d\Delta$, nondiffractive and diffractive, according to whether Δ is small or large, respectively. The separation improves with energy. We thus consider the operational definition of diffractive events as those where Δ is greater than some fixed quantity, on the order of the correlation length.

Considering first the nondiffractive component, we find it has the following general properties:

(1) $d\sigma/d\Delta$ is sharply peaked at low values of Δ, the peak occurring in the vicinity of $Y/\langle n\rangle$.

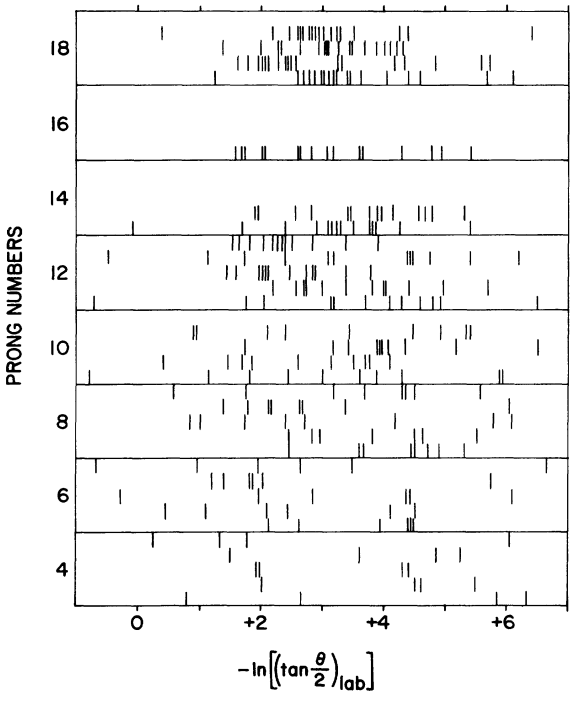

FIG. 1. $\ln\tan(\frac{1}{2}\theta)$ distribution for individual tracks from a sample of events of various multiplicities at 205 GeV/c.

(2) $d\sigma/d\Delta$ falls off exponentially for large Δ, with a slope related to the contributing Regge trajectory α_M:

$$\frac{d\sigma}{d\Delta} \sim e^{-(2-2\alpha_M)\Delta} .$$

(3) The curve is very slowly varying with energy, moving towards higher Δ values only as $\ln Y$.

In contrast, we find the diffractive components contribute to a wide range in Δ, with a peak at $\Delta = Y$ (the maximum possible Δ) resulting from single diffraction into low mass and the elastic cross section, if included. When both components are considered together, the crucial question is what energy is required for adequate separation of the two regions. We find, using simple models, that NAL energies are probably not sufficiently high enough, though CERN ISR energies may be. However, at any energy there will probably be an appreciable number of Pomeron-exchange events in the nondiffractive region.

Experimentally, it is easier to measure the variable $\eta = -\ln\tan(\frac{1}{2}\theta)$, which is similar but not identical to rapidity. The definitions of y and η are

$$y = \tfrac{1}{2}\ln\left(\frac{E+p_{\parallel}}{E-p_{\parallel}}\right),$$

$$\eta = \tfrac{1}{2}\ln\left(\frac{p+p_{\parallel}}{p-p_{\parallel}}\right) .$$

If rapidity is not available, one may use the maximum η difference distribution. However, there will be some loss of resolution so that higher energy is required to obtain the same separation of the two regions. Nevertheless, as an illustration of the effects we are considering, we shown in Fig. 1 the η plots of a sample of 31 events at 200 GeV/c.[3]

In Sec. II, we derive some properties of the distribution $d\sigma/d\Delta$. In Sec. III, we describe a particular multiperipheral model. We present the results and summarize in Sec. IV.

II. ANALYSIS OF $d\sigma/d\Delta$

Before looking at specific models, let us look at the general behavior we expect to find for $d\sigma/d\Delta$. Since rapidities are limited to the region $0 \lesssim y_i \lesssim Y$, we see that high-multiplicity events are less likely to have large gaps in rapidity. Similarly, since $Y \approx \sum_{i=2}^{n}(y_i - y_{i-1})$ we see that *low*-multiplicity events *must* have at least one large gap. In fact, the minimum Δ for n particles is $Y/(n-1)$, where $(n-1)$ is the number of gaps. The last statement neglects leading neutral particles; however, to the extent that there is a charged particle some-

where near the end of the rapidity interval, it follows that low-charged-multiplicity events do not give gaps appreciably smaller than $Y/(n-1)$. These kinematic considerations are helpful in analysis, but are less important than the dynamical effects we consider next. (Note that the *existence* of low-prong events at high energy is itself a dynamical result; i.e., without diffraction, low-prong cross sections vanish like a power of s as energy increases.)

A. Nondiffractive contribution

Before turning to a multiperipheral model for the analysis, we first illustrate the results with a simple Regge model. This involves examining the process as illustrated in Fig. 2. If Δ is the separation in rapidity of the two blobs M_1 and M_2, then for large Δ, M_1/m_a, M_2/m_b, we have

$$e^{\Delta} \approx \frac{-st}{M_1^2 M_2^2} \quad . \tag{3}$$

In the same large-Δ limit, the differential cross section looks like

$$\frac{d^3\sigma}{dM_1^2 dM_2^2 dt} \sim \left(\frac{-st}{M_1^2 M_2^2}\right)^{2\alpha_M(t)-2} \sim e^{\Delta[2\alpha_M(t)-2]} , \tag{4}$$

where $\alpha_M(t)$ is a meson Regge trajectory. We then expect the Δ distribution to fall off exponentially for large Δ, with a slope given by $(2\bar{\alpha}_M - 2)$, where $\bar{\alpha}_M$ is the effective α_M over the appropriate region in t. Since this region is generally small, it is a good approximation to say that

$$\frac{d\sigma}{d\Delta} \underset{\Delta \text{ large}}{\sim} ce^{\Delta[2\alpha_M(0)-2]} \quad . \tag{5}$$

Notice that this rate of decrease is the same as the rate at which exclusive cross sections decrease in s. This argument is only crudely correct, since the dependence of σ on M_1 and M_2 has been ignored.

In the framework of the multiperipheral picture, an instructive model for maximum-gap distributions is the one-dimensional version of the Chew-Pignotti model.[4] In this model the differential cross section,

$$s\frac{d^n\sigma}{dy_1 \cdots dy_n} = k(y_1)k(y_2 - y_1)\cdots \times k(y_n - y_{n-1})k(Y - y_n) , \tag{6}$$

is determined by the kernel

$$k(z) = ge^{(2\alpha_M - 1)z} \equiv ge^{\beta z} \quad . \tag{7}$$

The Laplace transform of (7) is

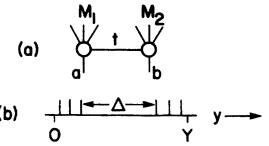

FIG. 2. Kinematic variables of a general Reggeized production amplitude.

$$K(J) = \frac{g}{J-\beta} ,$$

which is used to generate the full cross section. However, Eq. (1) requires that we obtain the transform of

$$k(\Delta, z) = ge^{\beta z}\theta(\Delta - z) ,$$

i.e.,

$$K(\Delta, J) = g\frac{1 - e^{-(J-\beta)\Delta}}{J-\beta} \quad . \tag{8}$$

The Δ-limited cross section, $\sigma(\Delta, s)$, is obtained from an "absorptive amplitude," $a(\Delta, s)$:

$$\sigma(\Delta, s) = \frac{1}{s}\, a(\Delta, s) .$$

The transform of $a(\Delta, s)$ is

$$A(\Delta, J) = g\sum_{n=0}^{\infty} K(\Delta, J)^{n+1} = \frac{gK(\Delta, J)}{1 - K(\Delta, J)} \quad . \tag{9}$$

The leading behavior of $\sigma(\Delta, s)$ is obtained from (9) by locating the leading zero of $1 - K(\Delta, \alpha(\Delta))$. The inverse transform (neglecting the residue and numerical factors) then yields $\sigma(\Delta, s) \sim s^{\alpha(\Delta)-1}$. It is easy to see that $\alpha(\Delta)$ should be bounded by unity. We see below that $\alpha(\Delta)$ is monotonically increasing with Δ. For large gaps, the behavior of $d\sigma/d\Delta \sim \alpha'(\Delta)(\ln s)s^{\alpha(\Delta)-1}$ depends upon $\alpha(\Delta)$ and $\alpha'(\Delta)$. To obtain the approximate behavior of $\alpha(\Delta)$, we note that the vanishing of $1 - K(\Delta, \alpha)$, i.e.,

$$\alpha - \beta - g(1 - e^{-(\alpha-\beta)\Delta}) = 0 ,$$

has the large-Δ solution

$$\alpha(\Delta) \sim \beta + g(1 - e^{-g\Delta}) . \tag{10}$$

Since $\alpha(\infty) = 1$ implies $g = 1 - \beta = 2 - 2\alpha_M$, for the maximum-gap distribution we obtain

$$\frac{d\sigma}{d\Delta} \sim e^{-(2-2\alpha_M)\Delta}(\ln s)s^{\alpha(\Delta)-1} . \tag{11}$$

Notice that $d\sigma/d\Delta$ is the product of an increasing and a decreasing function of Δ, and has a peak. Well above the peak, where $\alpha(\Delta) \cong 1$, Eq. (11) can be approximated by

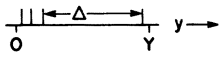

FIG. 3. Typical single-diffractive-dissociation event in rapidity space.

$$\frac{d\sigma}{d\Delta} \sim e^{-(2-2\alpha_M)\Delta} \ln s \ . \tag{12}$$

This shows the exponential decrease which was derived earlier [Eq. (5)]. We can also deduce from Eq. (12) that the distribution $d\sigma/d\Delta$ translates upwards in Δ at the rate of $\ln(\ln s)$ as $s \to \infty$. For large Δ, the quantity $(1/\ln s)(d\sigma/d\Delta)$ should be energy-independent.

B. Diffractive contribution

A typical *diffractive dissociation* event looks (in rapidity space) like the example in Fig. 3. This example shows diffraction into 3 and 1 particles, with a large gap Δ in between. We will now study the behavior of $d\sigma/d\Delta$ for diffractive events.

We first enumerate the various types of Pomeron (P) exchange we need to consider. We ignore multiple P exchange, leaving single or double diffractive dissociation (d.d.), i.e., single Pomeron exchange. We further distinguish between diffraction into low masses (the resonance region), and high masses ($\langle M \rangle \sim 5$ GeV at $P_{\text{lab}} = 200$ GeV/c). Low-mass single diffractive dissociation is equivalent to the g_{PPM} contribution in the inclusive single-particle distribution, while high-mass single d.d. is equivalent to the contributions from the triple Pomeron coupling, g_{PPP}. We will consider only single diffraction (both low and high mass), and double low-mass diffraction.

Our model for the low-mass diffractive dissociation will be a multiperipheral chain that generates an output pole at $\frac{1}{2}$, coupled to a Pomeron. The model for high-mass dissociation will be a multiperipheral model that generates an output pole at 1, coupled to a Pomeron. These models are shown

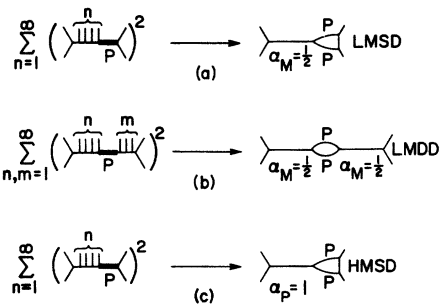

FIG. 4. (a) Diagrammatic model for low-mass single diffraction (LMSD). (b) Diagrammatic model for low-mass double diffraction (LMDD). (c) Diagrammatic model for high-mass single diffraction (HMSD).

in Fig. 4. If we assume the largest gap (z_2) is the Pomeron and use z_1 as the total rapidity across the dissociation products, single diffractive dissociation is given by

$$\frac{d\sigma}{d\Delta} \propto \frac{1}{s} \int dz_1 \int dz_2 \, e^{\alpha z_1} e^{(2\alpha_P - 1) z_2} \times \delta(z_2 - \Delta) \delta(Y - z_1 - z_2) = e^{(\alpha-1)Y} e^{(2\alpha_P - 1 - \alpha)\Delta} \ . \tag{13}$$

Taking $\alpha_P = 1$ and $\alpha = \frac{1}{2}$, then $d\sigma/d\Delta \sim e^{(\Delta - Y)/2}$, which increases with Δ whereas the nondiffractive part decreased. Since this contribution to $d\sigma/d\Delta$ is just a function of $Y - \Delta$, as s increases, this contribution translates to higher Δ at the rate $\ln s$. For high-mass single dissociation we put $\alpha = 1$ in Eq. (13) and the distribution is independent of both Δ and Y. (The integrated contribution is increasing like $\ln s$ but this is because the mass interval is increasing like $\ln s$.) For double dissociation (assuming both α's are the same), we get

$$\frac{d\sigma}{d\Delta} = \frac{1}{s} \int_0^{Y-\Delta} dz_1 \int_0^{Y-z_1} dz_3 e^{\alpha z_1} e^{(2\alpha_P - 1)\Delta} e^{\alpha z_3} \times \delta(Y - z_1 - \Delta - z_3) = (Y - \Delta) e^{(2\alpha_P - 1 - \alpha)\Delta} e^{(\alpha - 1)Y} , \tag{14}$$

which is again only a function of $Y - \Delta$, if $\alpha_P = 1$.

The important feature of the diffractive contribution is that asymptotically it "pulls apart" like $\ln s$ from the nondiffractive contribution, and is large at large Δ, where the latter is small.

One might fear that a large gap between two charged particles, resulting from emission of many neutral particles between them, would behave similarly to a gap caused by Pomeron exchange. However, if this were the case the prong cross sections (since they are summed over neutral particles) would not fall off as the energy increases. Since the prong cross section, summed over neutral particles, falls off approximately like $s^{-0.8}$, we expect that the nondiffractive part of the rapidity-gap distribution, summed over neutral particles, will fall approximately like $e^{-0.8\Delta}$ [see Eq. (5)], whereas the Pomeron-exchange part is constant or increasing in Δ.

III. NUMERICAL CALCULATIONS

Although the Chew-Pignotti model is useful in obtaining the qualitative predictions, one needs a more general model to do a quantitative calculation. We will start with the nondiffractive component and will treat it in greater detail since more is known about it.

We need a model which includes input singularities from Regge poles at $\frac{1}{2}$ (because this affects the falloff of $d\sigma/d\Delta$ at large Δ) and yet still gets

the average multiplicity correct. The Chew-Pignotti model cannot do this, so we turn to a slightly more general model, one that includes "resonances" via a δ function in the kernel.[5] The other effect that needs to be included is neutral-particle production. We thus introduce two coupling constants, for charged and neutral particles, g_{ch} and g_0, and will make a statistical-independence assumption. To have a 2:1 ratio of charged to neutral particles produced, we put $\frac{1}{2}g_{ch}=g_0=\frac{1}{3}g$. The kernel as a function of rapidity difference z (without a cutoff Δ) is

$$k(z)=(g_0+g_{ch})[e^{\beta z}+\lambda\delta(z)]\,, \tag{15}$$

or in the J plane

$$K(J)=(g_0+g_{ch})\left(\frac{1}{J-\beta}+\lambda\right)\,. \tag{16}$$

The last term can also be considered the limit of $\lambda\beta_L/(J+\beta_L)$ as $\beta_L\to\infty$, i.e., an input singularity low in the J plane. To fix the constants in the kernel we find the output pole and average multiplicity. We examine

$$\sum_{n=0}^{\infty}K(J)^{n+1}=\frac{K(J)}{1-K(J)}$$
$$=\frac{g[(J-\beta)\lambda+1]}{(J-\beta)(1-g\lambda)-g}\,. \tag{17}$$

This has a pole at $\alpha=\beta+g/(1-g\lambda)$ and an average multiplicity of

$$\langle n\rangle=B\ln s\,,$$

where

$$B=g\frac{\partial\alpha}{\partial g}$$
$$=\frac{g}{(1-g\lambda)^2}\,.$$

Taking $\beta\equiv 2\alpha_M-1=0.0$, $\alpha=1.0$, and $B=2.0$ fixes $g=\frac{1}{2}$ and $\lambda=1.0$. Hence $g_{ch}=\frac{1}{3}$ and $g_0=\frac{1}{6}$.

Temporarily writing $K(J)=K_0+K_{ch}$, then

$$\sum_{n=1}^{\infty}(K_0+K_{ch})^n=\frac{K_0+K_{ch}}{1-(K_0+K_{ch})}$$
$$=\frac{(K_0+K_{ch})/(1-K_0)}{1-K_{ch}/(1-K_0)}\,. \tag{18}$$

We note that

$$\frac{K_{ch}}{1-K_0}=K_{ch}+K_{ch}K_0+K_{ch}K_0^2+\cdots \tag{19}$$

is the "renormalized" propagator for getting from one charge to the next, summing over the neutral particles in between. We will call it K_r. It is this propagator that should be cut off:

$$K_r(J)=\frac{K_{ch}}{1-K_0}=\frac{g_{ch}+g_{ch}\lambda(J-\beta)}{(J-\beta)(1-g_0\lambda)-g_0}$$
$$=G\left(\frac{1}{J-\gamma}+\Lambda\right)\,, \tag{20}$$

where

$$G=\frac{g_{ch}}{(1-g_0\lambda)^2}=\frac{12}{25}\,,$$

$$\gamma=\beta+\frac{g_0}{1-g_0\lambda}=0.20\,,$$

and

$$\Lambda=\lambda(1-g_0\lambda)=\frac{5}{6}\,.$$

Now to cut off the kernel wherever the rapidity difference between *charged* particles exceeds Δ, we simply write [the $\delta(z)$ needs no cutoff]

$$K_r(J,\Delta)=G\left(\frac{1-e^{-(J-\gamma)\Delta}}{J-\gamma}+\Lambda\right)\,. \tag{21}$$

However, we have not yet considered the problem of neutral particles on the end of the chain. Since in this case no rapidity is measured across these neutral particles they require special treatment. That is, we want to allow the rapidity difference between an incoming particle and the nearest charged particle to be greater than Δ if it wishes. (This cannot be Pomeron exchange since it is charge exchange.) This sum over neutral particles is the same as before except the numerator is now one. So we have the factor

$$\frac{1}{1-K_0(J)}=1+\frac{K_0(J)}{1-K_0(J)}$$
$$=1+\tfrac{1}{2}K_r(J)\,. \tag{22}$$

The entire cross section is then generated by the amplitude

$$A(J,\Delta)=[1+\tfrac{1}{2}K_r(J)]\frac{K_r(J,\Delta)}{1-K_r(J,\Delta)}[1+\tfrac{1}{2}K_r(J)]\,. \tag{23}$$

Using a pole approximation we determined numerically the cross section $\sigma(\Delta, Y)$ corresponding to this amplitude. That is, we numerically determined the positions and residues of the (real) poles, both in $K_r(J)$ and in $[1-K_r(J,\Delta)]^{-1}$. The complex poles were found to contribute little at this energy for most Δ.

Next we turn to the calculation of the diffractive dissociation distribution. Because less is known about the diffractive component than the nondiffractive (for instance, $\langle n\rangle_D$ is not yet known), we will use the simpler Chew-Pignotti model discussed in Sec. II. Because we expect that only the single-diffractive (both high- and low-mass) and

possibly the double low-mass diffractive cross sections are important we limit our calculation to these. For the single diffraction (SD) we take (we also ignore complications due to neutral particles)

$$A_{\mathrm{SD}}=\frac{K_M(\Delta,J)}{1-K_M(\Delta,J)}K_P(\Delta,J).$$

M and P refer to meson and Pomeron exchange, respectively;

$$K_i=g_i\frac{1-e^{-(J-\beta_i)\Delta}}{J-\beta_i},\quad i=M\text{ or }P.$$

We used $\beta_P=1.0$ and $g_M=0.74$. The value of β_M depends on whether we are generating high- or low-mass diffraction and was chosen to make the zero of $1-K_M(\infty,J)$ be at $J=1.00$ or 0.5, respectively. That is, $\beta_M=0.26$ and -0.24 for high- and low-mass dissociation. None of the numerical values in this diffractive model have any particular significance, nor are the results sensitive to small variations in them.

To calculate the double low-mass d.d. (LMDD) we use the amplitude

$$A_{\mathrm{LMDD}}(\Delta,J)=\frac{K_M(\Delta,J)}{1-K_M(\Delta,J)}K_P(\Delta,J)\frac{K_M(\Delta,J)}{1-K_M(\Delta,J)}$$

with the same parameters as before. However, in this case it appeared simpler to use the transformed amplitude, so the numerical calculation was done using

$$\sigma_{\mathrm{LMDD}}(\Delta,s)=\sum_{n=2}^{\infty}\sigma^n_{\mathrm{LMDD}}(\Delta,s),$$

where

$$\sigma^n_{\mathrm{LMDD}}(\Delta,s)=(n-1)g_M{}^{n-2}g_P{}^2e^{(\beta_M-1)}\sum_{k=0}^{n}(-)^k\binom{n}{k}\left\{\sum_{i=0}^{n-1}\left[\frac{e^{\delta\Delta}\phi_k{}^{n-i-1}\theta(\phi_k)-\psi_k{}^{n-i-1}\theta(\psi_k)}{\delta^{i+1}(n-i-1)!}\right]+\frac{e^{\delta\psi_k}}{\delta^n}\theta(\psi_k)\theta(-\phi_k)\right\},$$

where

$$\phi_k=Y-(k+1)\Delta,$$

$$\psi_k=Y-k\Delta,$$

and

$$\delta=\beta_P-\beta_M.$$

IV. RESULTS

In Sec. III we described a simple model for the maximum-rapidity-gap distribution. This model contains a fairly detailed nondiffractive component, one designed to agree with the general features of the data. The diffractive component of the model is less detailed, but also contains the basic features of a reasonable model. Thus, we expect the model as a whole to describe adequately the general features of the data, though we do not expect it to agree in detail. In particular, the model cannot fit individual prong cross sections, and therefore we will not use it to predict $d\sigma^n/d\Delta$ distributions for a fixed number of prongs.

In Figs. 5 and 6 we show the distributions $d\sigma/d\Delta$ (unnormalized) predicted by our model for the various components, at $Y=6$ ($s\approx 400$ GeV^2). We

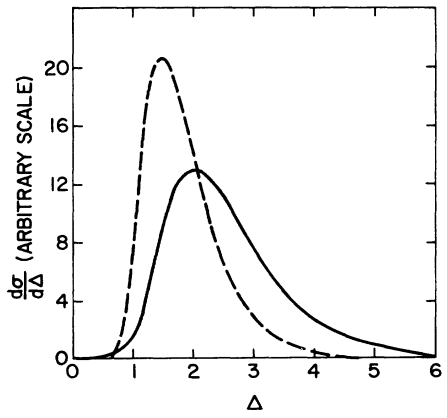

FIG. 5. Nondiffractive-model predictions for $d\sigma/d\Delta$ versus Δ, at $Y=6$. The solid curve is the prediction of the detailed model (see text); the dashed curve is from a simple Chew-Pignotti model ($\beta=-0.5$). The curves are normalized to $\sigma_{\mathrm{ND}}=27$ mb.

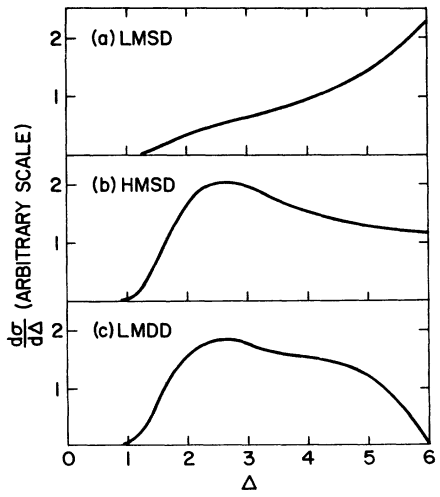

FIG. 6. Diffractive contributions to $d\sigma/d\Delta$ at $Y=6$. Normalization is arbitrary. (a) Low-mass single diffraction (LMSD). (b) High-mass single diffraction (HMSD). (c) Low-mass double diffraction (LMDD).

see the characteristic features predicted earlier, with some modifications. In particular:

(1) $(d\sigma/d\Delta)_{ND}$ peaks at low Δ and decreases at higher Δ.

(2) $(d\sigma/d\Delta)_{LMSD}$ peaks at $\Delta = Y$, and falls off rapidly with decreasing Δ.

(3) $(d\sigma/d\Delta)_{HMSD}$ is flat at high Δ. The hump at lower Δ arises from events where the largest gap, Δ, is *not* across the Pomeron.

(4) $(d\sigma/d\Delta)_{LMDD}$ increases for moderate Δ, then decreases to zero at $\Delta = Y$. The excess of events at lower Δ is again due to the largest gap being a meson trajectory rather than the Pomeron.

In Fig. 5 we also show (dashed line) the nondiffractive contribution which would result from a simple Chew-Pignotti model with input pole at 0.25. We see that this lower pole produces a much narrower distribution. The two nondiffractive models probably cover the range of reasonable models. The following discussion concerns the model of Sec. III, but comparison to the dashed curve will help define the range of possible effects. Clearly, the narrower curve allows the better separation of events.

The normalizations of the various components of the cross section are not well known. In order to arrive at some idea as to the shape of the overall distribution, however, we make the following reasonable guess (at $Y = 6$):

$$\begin{aligned} \sigma_{ND} &= 27 \text{ mb}, \\ \sigma_{LMSD} &= 4.5 \text{ mb}, \\ \sigma_{HMSD} &= 1 \text{ mb}, \\ \sigma_{LMDD} &= 0.7 \text{ mb}. \end{aligned} \tag{24}$$

The value of σ_{ND} is typical of those quoted experimentally.[6] If we take $\sigma_{el} = 6.8$ mb and $\sigma_T = 40$ mb, we arrive at $\sigma_D = 6.2$ mb. The value of 1 mb for σ_{HMSD} is rather uncertain, but agrees roughly with estimates made by Frazer and Snider.[6] This quantity is, however, quite model-dependent, and could, in fact, be zero. With σ_{HMSD} fixed at 1 mb and σ_D at 6.2 mb, the σ_{LMSD} and σ_{LMDD} are determined by factorization:

$$\sigma_{el} = \frac{(\frac{1}{2}\sigma_{LMSD})^2}{\sigma_{LMDD}} .$$

As we increase the energy, only σ_{HMSD} increases, as $\ln s$, since the high-mass region is increasing.

With these guidelines, we have plotted in Figs. 7 and 8 the distribution $d\sigma/d\Delta$, summed over all contributions, for $Y = 6$ and 8, respectively. The dashed lines in each figure give the total diffractive and nondiffractive components.

It is evident from Fig. 7 that the nondiffractive component dominates the distribution up to $\Delta \sim 4.5$.

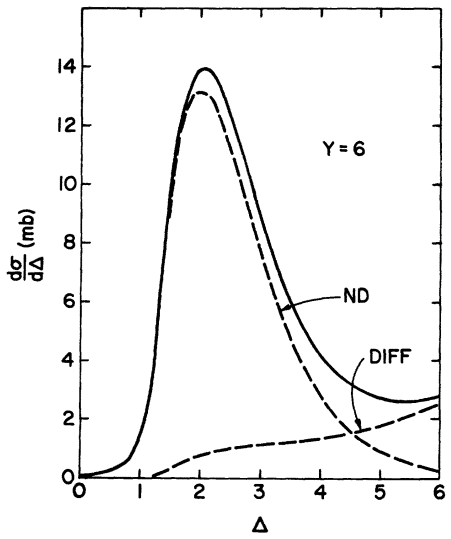

FIG. 7. Model predictions for $d\sigma/d\Delta$ at $Y = 6$. Dashed curves show the nondiffractive and diffractive contributions with normalizations from Eq. (24).

The diffractive component lies largely under the nondiffractive peak, and there is only slight evidence of a peak at $Y = \Delta$. One approach to utilizing such a distribution (the solid line) would be to make a cut at $\Delta = 4.5$. If we do this, we see that roughly 75% of the large-Δ events are diffractive, while one-half of the diffractive events lie below $\Delta = 4.5$. Thus, the separation of diffractive from nondiffractive events will be quite difficult. More refined techniques, such as fitting the curves to exponentials, may work better, with sufficient data. Note that the low-Δ diffractive events are almost entirely from high-mass diffraction. It

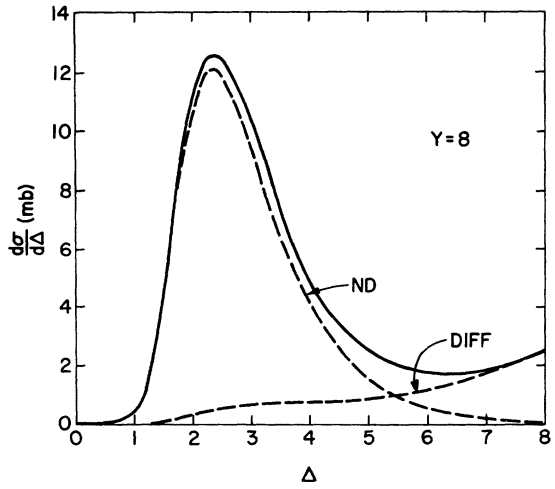

FIG. 8. Model predictions for $d\sigma/d\Delta$ at $Y = 8$. Dashed curves show the nondiffractive and diffractive contributions with normalizations from Eq. (24).

appears that such events, if they do exist, will be very difficult to locate by using $d\sigma/d\Delta$.

At $Y=8$, the situation is somewhat improved. Taking only events with $\Delta \geq 5$ would get $\frac{2}{3}$ of the diffractive events, with about a 20% contamination of nondiffractive events. Again, the high-mass diffractive contribution is mostly missed.

We should temper these pessimistic statements by pointing out the conservative nature of the model we have chosen. We have used only the highest possible meson trajectory, which gives the slowest decrease in $(d\sigma/d\Delta)_{ND}$. Equivalently (through duality), actual resonances take up a nonvanishing amount of rapidity, in contrast to our δ-function term, reducing the gap size for nondiffractive events. Thus we can state that a more realistic model can and probably will have a narrower nondiffractive distribution, thus improving the separation of events. For example, the narrower distribution $(d\sigma/d\Delta)_{ND}$ of Fig. 5 would yield a total distribution with a separation around $\Delta=3.5$, rather than at 4.5. We regard this model as the most optimistic possibility, and expect the true physics to be somewhere in between the two models discussed here.

The $d\sigma/d\Delta$ analysis can be improved by making additional cuts on the data. For instance, requiring that the charge exchanged across the largest gap be zero will eliminate some nondiffractive events in the large-Δ region. Similarly, if one wishes to look at double dissociation, the requirement must be made that the largest gap not appear at the end of the rapidity interval (i.e., with only the proton at one end of the gap). Such analysis will improve the isolation of diffractive from nondiffractive events.

It has been suggested that diffractive dissociation be *defined* as large gaps in rapidity. The standard definition is that diffractive dissociation means Pomeron exchange. Our analysis shows that at 200 GeV/c, or even 1500 GeV/c, the definitions still differ considerably. It appears that if one wants to determine the amount of Pomeron exchange, the $d\sigma/d\Delta$ distribution (at one energy) is certainly less useful than energy-dependent triple-Regge fits, but perhaps as useful as the standard energy-independent analysis of diffractive dissociation from missing-mass distributions.[7]

ACKNOWLEDGMENTS

We wish to acknowledge numerous discussions with and several suggestions by Gerald Thomas. We also wish to thank Richard Singer for preliminary examination of the 205-GeV/c data. Finally we wish to thank Argonne Laboratory for their hospitality, and for financial support from the HEP Division (D. R. S.) and the Argonne Center for Educational Affairs (S. T. J.). One of us (S. T. J.) wishes also to thank the Research Corporation for support during preliminary phases of this research.

---

*Work performed under the auspices of the U. S. Atomic Energy Commission.

†On summer leave from the Department of Physics, University of Alabama, University, Alabama.

‡Research supported in part by the Research Corporation.

§On summer leave from the Department of Physics, University of Wisconsin, Milwaukee, Wisconsin.

[1]H. D. I. Abarbanel, G. F. Chew, M. L. Goldberger, and L. M. Saunders, Ann. Phys. (N.Y.) 73, 156 (1972); G. F. Chew and S. D. Ellis, Phys. Rev. D 6, 3330 (1972); G. F. Chew, Phys. Rev. D 7, 934 (1973); D 7, 3525 (1973); W. R. Frazer, D. R. Snider, and C.-I Tan, Phys. Rev. D 8, 3180 (1973).

[2]Such an analysis of the 205-GeV/c bubble chamber data has been presented by R. Singer at the A.P.S. Berkeley High Energy Physics Conference, ANL report, August, 1973 (unpublished).

[3]J. Whitmore, in *Proceedings of the XVI International Conference on High Energy Physics, Chicago-Batavia, Ill., 1972*, edited by J. D. Jackson and A. Roberts (NAL, Batavia, Ill., 1973), p. 224.

[4]G. F. Chew and A. Pignotti, Phys. Rev. 181, 1914 (1969).

[5]S. Pinsky, D. R. Snider, and G. H. Thomas, ANL Report No. HEP 7349 (unpublished).

[6]W. R. Frazer and D. R. Snider, Phys. Lett. B45, 136 (1973).

[7]For example, see S. J. Barish *et al.*, ANL Report No. HEP 7338 (unpublished).